applied sciences

MDPI

Article

Mechanical and Tribological Characterization of a Bioactive Composite Resin

Elsa Reis Carneiro [1], Ana Sofia Coelho [1,2,3,4,*], Inês Amaro [1], Anabela Baptista Paula [1,2,3,4], Carlos Miguel Marto [2,3,4,5], José Saraiva [1], Manuel Marques Ferreira [2,3,4,6], Luís Vilhena [7], Amílcar Ramalho [7] and Eunice Carrilho [1,2,3,4]

1 Faculty of Medicine, Institute of Integrated Clinical Practice, University of Coimbra, 3000-075 Coimbra, Portugal; elsacreiscarneiro@gmail.com (E.R.C.); ines.amaros@hotmail.com (I.A.); anabelabppaula@sapo.pt (A.B.P.); ze-93@hotmail.com (J.S.); eunicecarrilho@gmail.com (E.C.)
2 Area of Environment, Genetics and Oncobiology (CIMAGO), Faculty of Medicine, Institute for Clinical and Biomedical Research (iCBR), University of Coimbra, 3000-548 Coimbra, Portugal; mig-marto@hotmail.com (C.M.M.); m.mferreira@netcabo.pt (M.M.F.)
3 CNC.IBILI Consortium, Faculty of Medicine, University of Coimbra, 3000-548 Coimbra, Portugal
4 Centre for Innovative Biomedicine and Biotechnology (CIBB), University of Coimbra, 3000-548 Coimbra, Portugal
5 Faculty of Medicine, Institute of Experimental Pathology, University of Coimbra, 3000-548 Coimbra, Portugal
6 Faculty of Medicine, Institute of Endodontics, University of Coimbra, 3000-075 Coimbra, Portugal
7 Centre for Mechanical Engineering, Materials and Processes (CEMMPRE), Department of Mechanical Engineering, University of Coimbra, 3030-788 Coimbra, Portugal; luisvilhena@gmail.com (L.V.); amilcar.ramalho@dem.uc.pt (A.R.)
* Correspondence: anasofiacoelho@gmail.com

Citation: Carneiro, E.R.; Coelho, A.S.; Amaro, I.; Paula, A.B.; Marto, C.M.; Saraiva, J.; Ferreira, M.M.; Vilhena, L.; Ramalho, A.; Carrilho, E. Mechanical and Tribological Characterization of a Bioactive Composite Resin. *Appl. Sci.* **2021**, *11*, 8256. https://doi.org/10.3390/app11178256

Academic Editor: Alessandro Ruggiero

Received: 16 August 2021
Accepted: 3 September 2021
Published: 6 September 2021

Abstract: Despite developments and advances in dental materials which allow for greater restorative performance, there are still challenges and questions regarding the formulation of new compositions and chemical reactions of materials used in restorative dentistry. The aim of this study was to assess and compare the mechanical and tribological characteristics of a bioactive resin, a composite resin, and a glass ionomer. Twenty specimens of each material were divided into two groups: one control group (n = 10), not subjected to thermocycling, and one test group (n = 10) submitted to thermocycling. The Vickers microhardness test was carried out and surface roughness was evaluated. The tribological sliding indentation test was chosen. The bioactive resin had the lowest hardness, followed by the composite resin, and the glass ionomer. The bioactive resin also showed greater resistance to fracture. For the tribological test, the wear rate was lower for the bioactive resin, followed by the composite resin, and the glass ionomer. The bioactive resin presented a smooth surface without visible cracks, while the other materials presented a brittle peeling of great portions of material. Thus, the bioactive resin performs better in relation to fracture toughness, wear rate and impact absorption than the composite resin and much better than the glass ionomer.

Keywords: restorative dentistry; bioactive resin; mechanical tests; friction behavior; wear mechanisms; thermocycling

1. Introduction

The ideal adhesive dental restorative material should have all the advantages of glass-ionomer systems combined with those of resin-based composites. It should be able to present superior wear resistance, as in a glass-ionomer system, and eventually also eliminate hydrolytic degradation of the adhesive interface, post-operative hypersensitivity, and polymerization shrinkage of composite resin systems [1,2].

The concept of dental restorative materials with bioactive properties arose from the combination of adhesive dentistry concepts and an understanding of fluoride's ability to prevent secondary or recurrent decay [2,3]. These materials are based on the development

of a layer with an affinity for apatite in the presence of an inorganic phosphate solution [2]. These bioactive materials also present numerous advantages, such as reduced polymerization shrinkage, a capacity for remineralization, induction of hydrophilicity, and intimate contact with dentin. In addition, they enable minimal formation of spaces between layers and are less technique sensitive than composite resins [2–6].

Activa™ BioActive restorative (Pulpdent, Watertown, MA, USA) and Activa™ BioActive base/liner (Pulpdent, Watertown, MA, USA) are the first bioactive dental materials with an ionic resin matrix and bioactive fillers that mimic some physical and chemical properties of natural teeth [7,8]. This bioactive material is believed to be an advance in the field of restorative dentistry as it combines improved physical properties and esthetics of composite resin systems together with all the benefits of resin-modified glass ionomers, such as the release and recharge of ions which can stimulate mineralization [6,8,9]. Conventional glass-ionomer cements also have bioactive properties, promoting remineralization of the tooth structure [2]. In addition, they do not need application of any extra products for retention or adhesion to dental hard tissues as composite resins do [2]. Moreover, this material is less technically demanding [10].

Despite the developments and advances in dental materials allowing for greater restorative performance, there are still challenges and questions regarding the formulation of new compositions and the chemical reactions of materials used in restorative dentistry [2]. Furthermore, it is challenging to find a dental restorative material that can withstand existing mechanical, chemical, and thermal stresses in the oral cavity while maintaining a high longevity rate [11]. Defining and comparing the physical and tribological properties of these materials allows for a correct and insightful selection of materials, depending on the needs of each particular case [12].

The aim of the present research paper is to assess and compare the mechanical and tribological characteristics of three different materials: a bioactive resin (Activa™ BioActive Restorative™, Watertown, MA, USA), a composite resin, and a glass ionomer, before and after thermocycling. The null hypothesis is that the bioactive resin does not perform better than the other two materials.

2. Materials and Methods

Activa™ Bio-active Restorative™ (Watertown, MA, USA), Filtek Supreme™ XTE (3M ESPE, St. Paul, MN, USA), and Ketac™ Fil Plus Aplicap™ (3M ESPE, St. Paul, MN, USA) were used.

Sixty parallelepipedal specimens (3 mm × 6 mm × 45 mm) were produced using a 3D printed rubber-like mold (twenty of each dental material). The mold was placed on a glass slab and filled manually, in one increment, with a slight excess of material and covered with another glass slab. Before curing, the resin samples were manually compacted by applying finger pressure on the upper glass slab to allow flushing of the excess material and to obtain smoother surfaces. The specimens that required a light cure were then photopolymerized using a light polymerizing unit Bluephase® (Ivoclar Vivadent AG, Schaan, Liechtenstein) with a light intensity of 1500 mW/cm^2 ± 10% for 40 s.

The composite material was polished in LaboPol-5 equipment (Struers, Ballerup, Denmark) using several SiC abrasive papers with 340, 600, 1000, and 2500 grit, with a continuous passage of water, until minimal visible imperfections were reached. When an abrasive paper was changed, the specimens were rotated by approximately 90° to eliminate the scratches created by the previous abrasive paper.

The specimens of each material were divided into two groups: one control group (n = 10), not subjected to thermocycling, and one test group (n = 10) submitted to 5000 cycles of thermocycling with a temperature variation of 5 °C to 55 °C for 60 s. The mechanical properties of the material were studied before and after the thermocycling cycles. The Vickers microhardness test was carried out and surface roughness was also evaluated. The tribological sliding indentation test was chosen.

2.1. Surface Microhardness

The microhardness measurement was performed using a Struers Duramin durometer (Struers, Ballerup, Denmark) according to the ASTM E384-10 standard [13]. This device has a maximum resolution of 0.01 µm, and hardness measures. It performs micro- and macrohardness measurements, with an applied load range between 10–2000 gf and has an automatic load exchange system. The positioning of the specimen is carried out by a micrometric measuring table with two degrees of freedom. In this study, the Vickers hardness (HV) value was determined by applying a load of 200 gf (1.962 N) for a dwell time of 40 s. For each specimen, the average of five indentations was determined and for each group of composites the average of the ten averages was calculated, before and after thermocycling.

2.2. Surface Roughness

In order to characterize the surface roughness of the different materials under investigation, several roughness parameters were evaluated using a Mitutoyo Surftest SJ 500P profilometer (Mitutoyo Co., Kawasaki, Japan). This device has an extendable arm and a stylus tip at its end that consists of a conical diamond with a tip radius of 5 mm and 60 degrees. The specimens are placed on the profilometer platform so that the diamond tip travels across the surface of the sample during its movement. This instrument is connected to a computer and controlled via the Formtracepak software (Mitutoyo, Aurora, IL, USA). As a means of removing shape deviation and waviness, the roughness profile (R-profile) was isolated using a cut-off wavelength λc filter. Surface roughness measurements—R_a (arithmetical mean roughness), R_z (mean roughness depth), R_q (root mean square) and R_{sk} (roughness skewness)—were in accordance with DIN/ISO standards, with 2D roughness parameters being calculated according to EN ISO 4287 [14].

2.3. Flexural Test

A four-point flexural test was performed in accordance with ASTM D 6272-02 [15]. This technique has already been used in previous research works [12]. In this type of four-point bending test, the moment between the internal supports remains constant with the consequence that only tractive and compressive stresses act along the cross section. Figure 1 shows a schematic picture of the two supports and the loading points as well the load span that is one half of the support span.

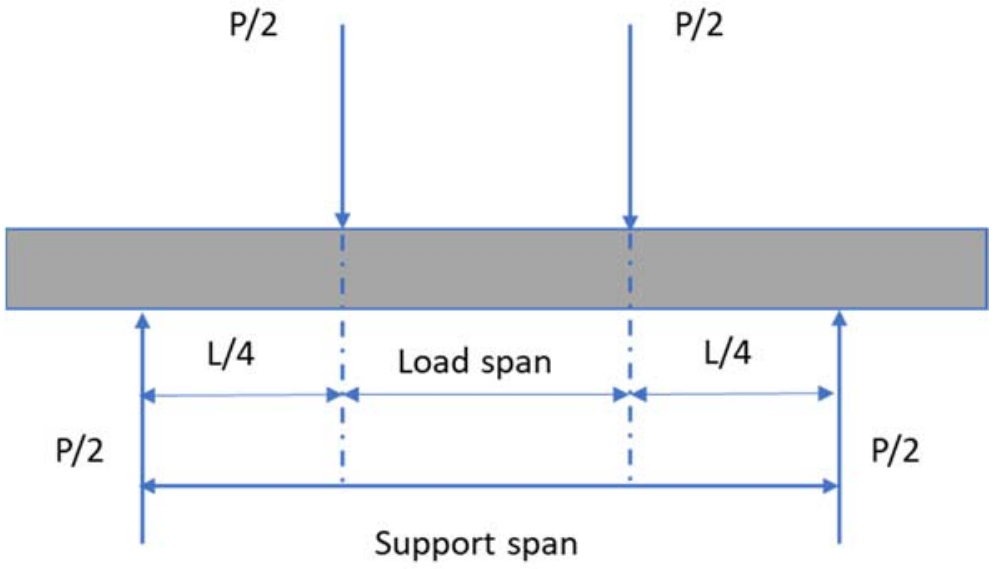

Figure 1. Schematic picture of the four-point bending test.

For this propose, a properly calibrated Shimadzu Autograph AG-X-5kN universal testing machnine (Shimadzu, Kyoto, Japan) was used (Figure 2). It was operated at a constant rate of crosshead motion of 0.5 mm/min using a support lower span of 40 mm and an upper loading span of 20 mm. At least five specimens (out of approximately ten) were used for each condition as stated in the standard. Before the tests, a muffle was used to maintain the temperature at the desired level with each specimen transported on a ceramic plate to maintain a constant temperature and then tested at a chosen temperature of 37 ± 2 °C.

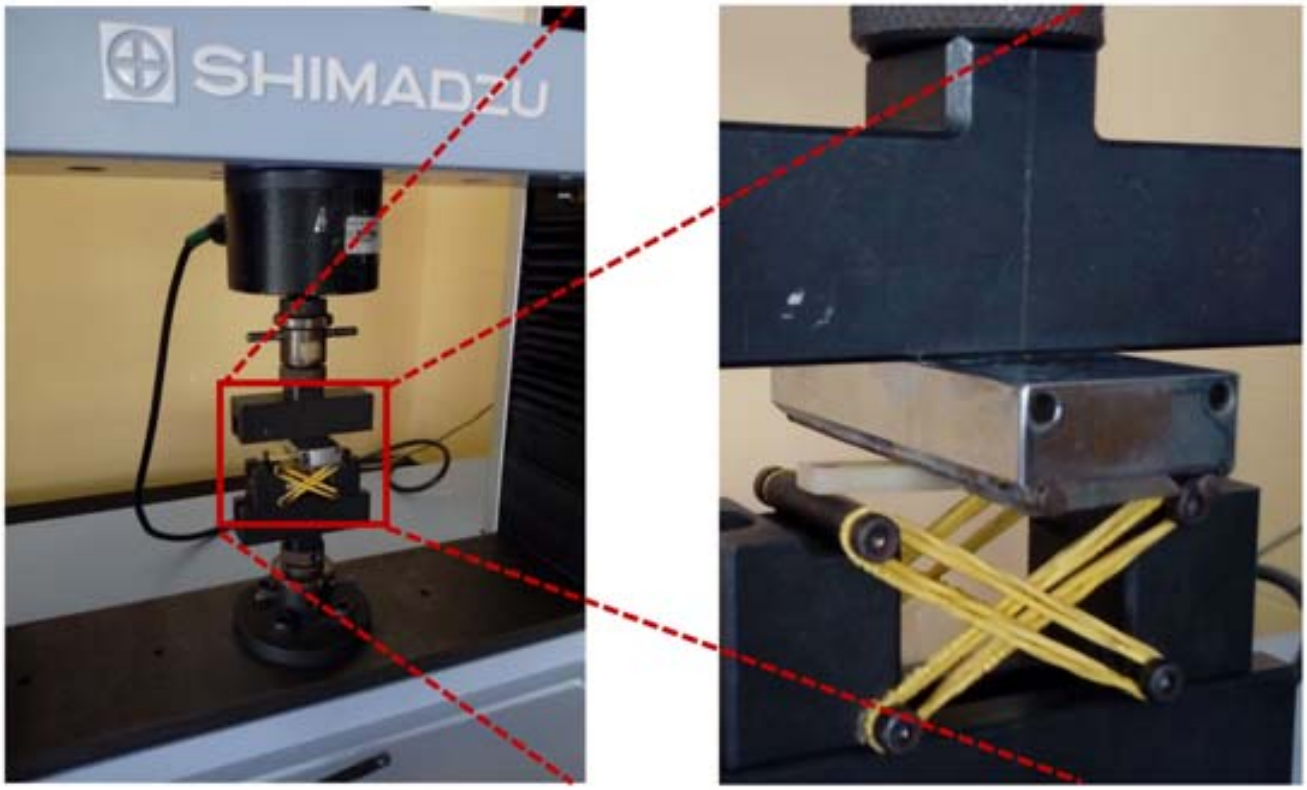

Figure 2. The four-point bending test configuration in the Shimadzu universal testing machine.

To carry out this test, the different specimens were submitted to flexure, as exemplified in the scheme presented in Figure 2, until failure was reached. The flexural test consists of applying a certain increasing load and monitoring the corresponding deflection. By analyzing the corresponding stress–strain curve, the various flexural properties were calculated. As stated in ASTM D6272-02 [15], the flexural strength (S) corresponds to the maximum stress reached at the moment of the break and is normalized through the section area using Equation (1). The static Young's modulus (E_S) is calculated using Equation (2). Finally, the work of fracture (WOF) or energy absorbed to fracture is calculated by the integration of the area of the stress–strain curve and provides a measure of the fracture toughness.

$$S = \frac{3PL}{4dt^2} \quad (1)$$

$$E_s = \left(\frac{P}{\delta}\right)\left(\frac{L^3}{bd^3}\right) \quad (2)$$

where: (P/δ) is the slope of the stress–strain curve in the elastic domain (N/mm), L is the support span (mm), d is the width of the specimen (mm) and t is the thickness of the specimen (mm).

2.4. Dynamic Young's Modulus

The dynamic Young's modulus was determined by impulse excitation of vibration technique described in the ASTM E 1876-01 [16]. This test method measures the fundamental resonant frequency of test specimens of suitable geometry by exciting them mechanically with an impulse tool, as shown in the flowchart of Figure 3. A ceramic piezoelectric transducer that is sensitive to a certain mechanical stimulus such as mechanical vibration was used and generates a potential difference when it undergoes a certain deformation. The signal analysis system is a digital oscilloscope connected to a laptop computer that uses the PicoScope 6 software (Pico® Technology, St. Neots, UK). Subsequently, using the OriginPro 2015 (OriginLab®, Northampton, MA, USA) program, a signal analysis was performed using a fast Fourier transform (FFT). By knowing the resonant frequency of a given specimen as well as its dimensions and mass, it was possible, using Equation (3), to determine the dynamic Young's modulus.

$$E_d = 0.9465 \left(\frac{m f_f^2}{b}\right)\left(\frac{L^3}{t^3}\right) T_1 \quad (3)$$

where: E_d is the dynamic Young's modulus (Pa), m the mass of the specimen (g), f_f the fundamental resonant frequency (Hz), t the thickness (mm), b the width (mm) and L the length of the specimen (mm). T_1 is a correction factor that depends on the geometry of the specimen that was set equal to the unity, for the specimen dimensions used in the current work.

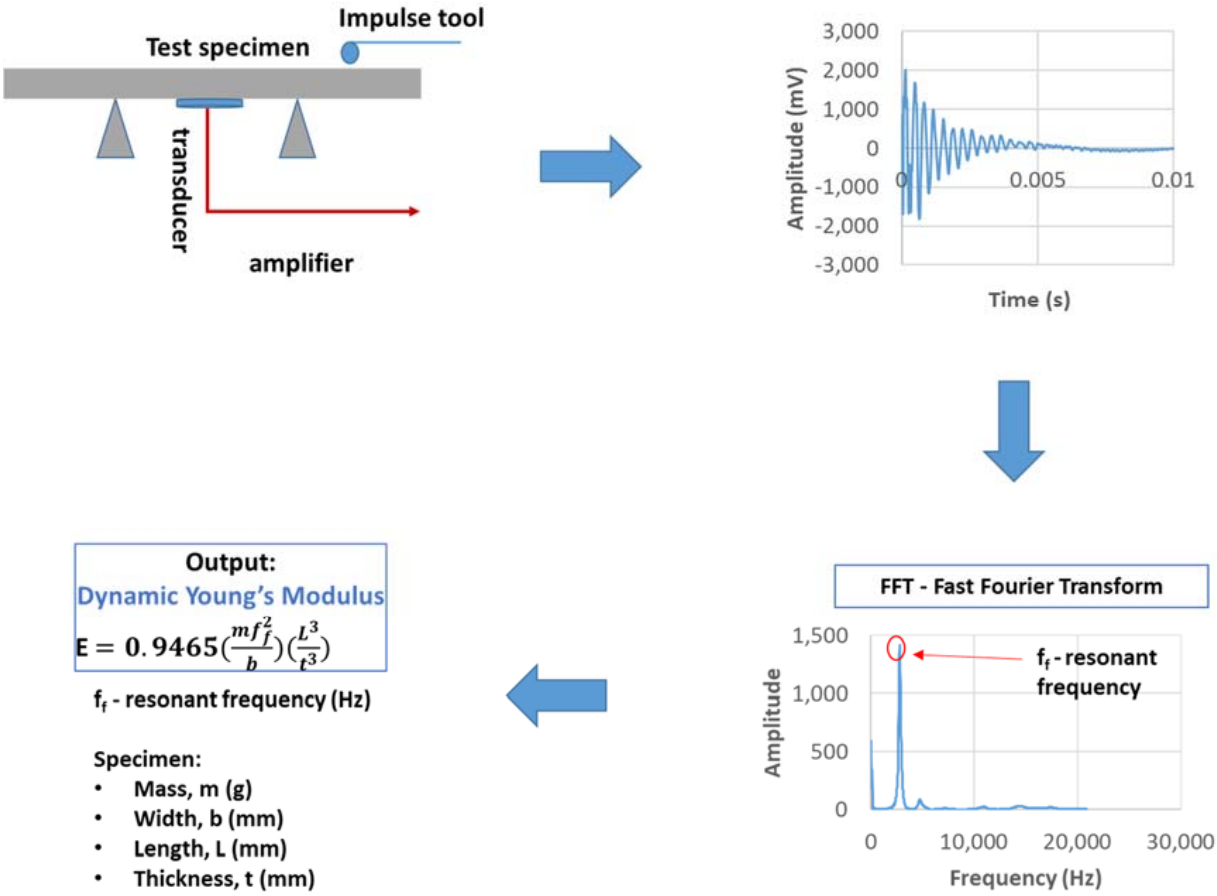

Figure 3. Flowchart of the experimental protocol used to measure the dynamic Young's modulus using the impulse excitation of vibration technique (the graphs show a real test for the Activa™ specimen after thermocycling).

Before the exciting impulse, all the specimens were heated in an oven, Digitheat (Selecta, Barcelona, Spain), at 40 °C for 1 h. Each specimen was removed one by one from the oven and transported on a ceramic plate and tested immediately at a temperature of 37 ± 2 °C. For each specimen, five determinations of the Young's modulus were achieved in order to estimate the mean and standard deviation.

The ratio of the loss modulus to storage modulus (E''/E') in a viscoelastic material is defined as the tan δ and provides information on the stress response under oscillatory deformation. This value was determined according to the following method, already used in previous papers [17]:

The logarithmic decrement, Δ can be calculate using Equation (4).

$$\Delta = \frac{1}{j} ln\left(\frac{Xi}{Xi+j}\right) = \zeta w_n T_a \quad (4)$$

where: X_i and X_{i+j} are the amplitude of two peaks of the free vibrating system, separated by j oscillations, ζ the damping factor, w_n the system vibratory frequency and T_a the average period of the wave form that can be calculated through Equation (5).

$$T_a = \frac{2\pi}{w_d} = \frac{2\pi}{w_n\sqrt{1-\zeta^2}} \quad (5)$$

where w_d is the dumped frequency of the system. Considering Equations (4) and (5), the logarithmic decrement, Δ is as follows:

$$\Delta = \frac{2\pi\zeta}{\sqrt{1-\zeta^2}} \quad (6)$$

For light dumping, Equation (6) can be simplified as follows (Equation (7)):

$$\Delta = 2\pi\zeta \quad (7)$$

From Equations (4)–(7), the damping factor ζ can be obtained and finally tan δ can be obtained as 2ζ.

2.5. Tribological Characterization

In order to carry out a tribological characterization of the different materials and measure the friction coefficient as well as the wear volume, the sliding indentation technique, or "scratch test", was used in accordance with ASTM G 171-13 [18]. This technique consists of scratching a specimen with a specific indenter of tungsten carbide with a 50 µm rounded tip and 60° conical shape. The specimen was fixed on a CNC sliding table with four axes and was moved with a speed of 0.5 mm/s according to the direction of the sliding line. An increasing load between 0 and 20 N was applied to the specimen surface, by the indenter, via a helical spring drive by linear actuator which allows for fast, high precision control (accuracy of 1 µm). A concomitant sliding movement of 10 mm was imposed by a second linear driver, with similar accuracy to that used to apply the load, connected to the lower specimen. A three-component load cell directly connected to the specimen was used to measure both normal and friction forces. The diagram in Figure 4 shows an example of a scratch test. Subsequently, the coefficient of friction was determined considering the slope of the curve between the tangential force vs. normal force and the plastic deformation caused by the indenter was analyzed and quantified using a profilometer. The wear mechanisms were observed by examining the wear track using a scanning electron microscope (SEM) (Hitachi-SU-3800, Hitachi, Japan) and an optical microscope (LEICA DM 2500, Leica, Germany).

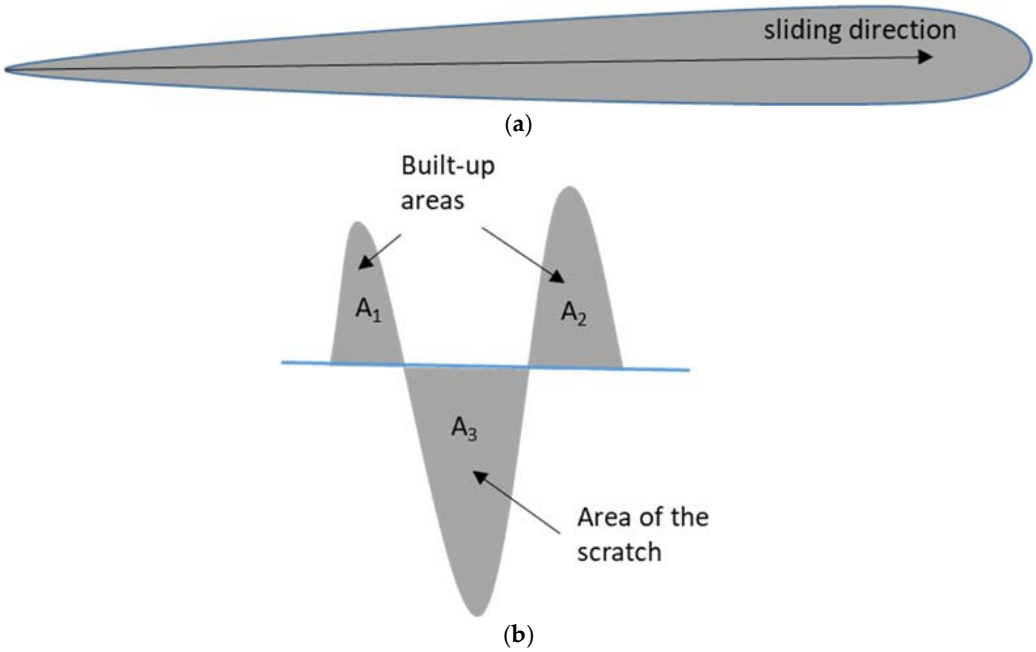

Figure 4. Schematic illustration of the wear track caused by the scratch test: (**a**) top view, showing the gradual area increase due to the load increase in the sliding direction; (**b**) cross-section view, showing the built-up areas (A1 + A2) and area of the scratch (A3).

After performing all the tribological tests using the sliding indentation technique for the characterization of the different specimens, before and after thermocycling, the respective coefficients of friction (COF) and wear were evaluated. Wear was evaluated by measuring the straight section profile of the wear track using a profilometer and measuring for a sliding distance of 8 mm and corresponding to an applied load of 16 N. The values of depth and worn area (A_3) were extracted from each wear track profile since the built-up areas corresponding to A_1 and A_2 were ignored as they did not present significant material accumulation.

2.6. Statistical Analysis

The results were initially evaluated descriptively, using the mean and the standard deviation. The Wilcoxon–Mann–Whitney test and the Kruskal–Wallis test followed by the Mann–Whitney U test using Bonferroni correction were used. The level of significance adopted throughout the statistical analysis was 5%. The software used in data processing was IBM®SPSS® v.28.0 (IBM Corporation, Armonk, NY, USA).

3. Results

3.1. Microhardness

The initial and final microhardness values and respective standard deviation for each material are shown in Figure 5. The Vickers hardness was significantly different among all groups ($p < 0.05$).

3.2. Roughness

The roughness results were represented by the different variables considered in the study: R_a, R_q, R_z and R_{sk} (Table 1).

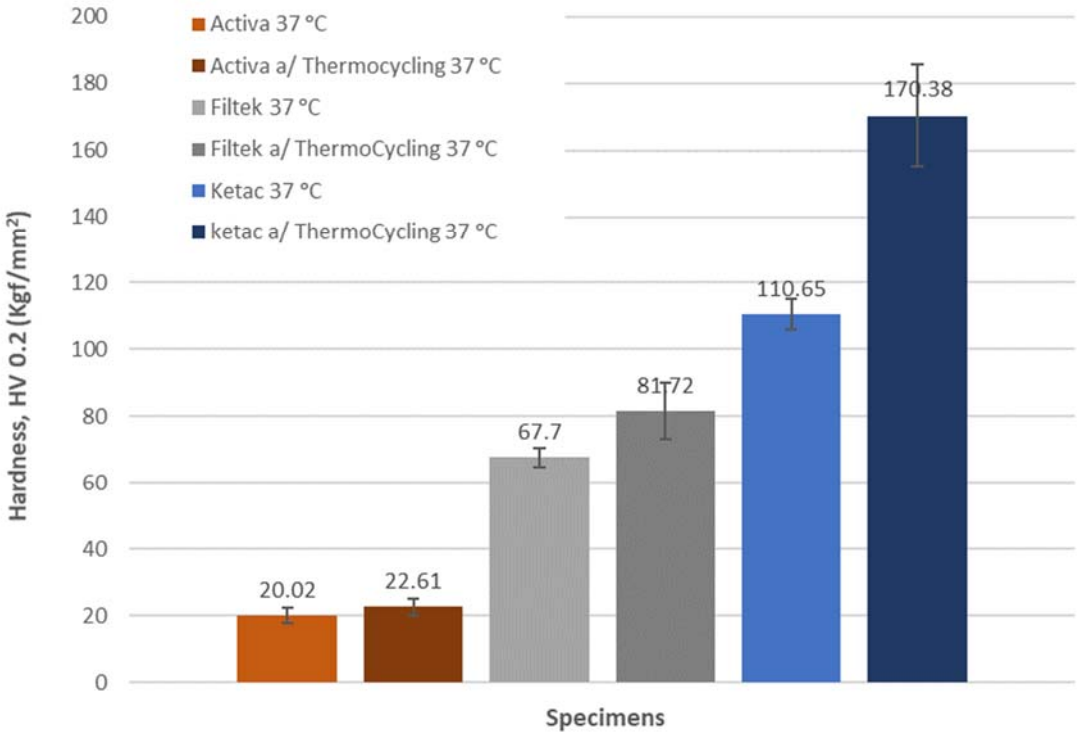

Figure 5. Hardness measurements, $HV_{0.2}$ for the three different materials (Activa™, Filtek Supreme™ XTE and Ketac™) before and after thermocycling (37 ± 2 °C).

Table 1. 2D roughness parameters, R_a, R_q, R_z and R_{sk} for the different materials before (37 ± 2 °C) and after thermocycling (37 ± 2 °C).

Material	Thermocycling	R_a (μm)	R_q (μm)	R_z (μm)	R_{sk} (μm)
Activa™	Before	0.26 ± 0.05	0.35 ± 0.08	2.08 ± 0.45	−0.87 ± 0.83
	After	0.52 ± 0.14	0.77 ± 0.23	3.25 ± 0.59	−0.07 ± 0.78
Filtek Supreme™ XTE	Before	0.30 ± 0.09	0.40 ± 0.14	1.41 ± 0.25	−0.09 ± 0.48
	After	0.17 ± 0.04	0.22 ± 0.07	1.23 ± 0.38	−0.31 ± 0.95
Ketac™	Before	0.36 ± 0.08	0.51 ± 0.15	2.35 ± 0.63	−1.45 ± 1.14
	After	0.78 ± 0.35	1.10 ± 0.55	4.17 ± 1.43	−1.08 ± 1.14

Before thermocycling, R_a and R_q presented similar results for the different materials. After thermocycling, these parameters showed a greater dispersion of results. Concerning R_z, a large dispersion between the results of the different specimens was observed, which increased after thermocycling, with Ketac™ having the highest results.

When comparing Filtek Supreme™ and Ketac™, statistically significant differences were found in the initial evaluation of R_a ($p = 0.012$), R_q ($p = 0.005$), R_z ($p = 0.003$), and R_{sk} ($p < 0.001$). After thermocycling, significant differences were found regarding R_a ($p = 0.002$), R_q ($p = 0.002$), and R_z ($p = 0.028$).

For Filtek Supreme™ and Activa™, statistically significant differences were found for the initial evaluation of R_z ($p < 0.001$) and R_{sk} ($p < 0.001$). After thermocycling, significant differences were found regarding R_a ($p = 0.028$), R_q ($p = 0.024$), and R_z ($p = 0.040$).

For Activa™ and Ketac™, statistically significant differences were found for the initial evaluation of R_a ($p = 0.022$) and R_q ($p = 0.042$). After thermocycling, no statistically significant differences were found.

Regarding R_{sk}, no statistically significant differences between groups were found after thermocycling ($p = 0.151$).

3.3. Flexural Test

The four-point flexural test allowed various mechanical properties to be calculated, such as flexural strength (S), static elastic modulus (E_s), and work of fracture (WOF).

The flexural strength (S) is illustrated in Figure 6. These results dropped monotonically with increasing temperature and after being subjected to thermocycling, reaching values of 36.58 MPa and 37.90 MPa for Activa™ and Filtek Supreme™, respectively. As for Ketac™, it was not possible to measure its flexural strength after thermocycling since the samples broke immediately.

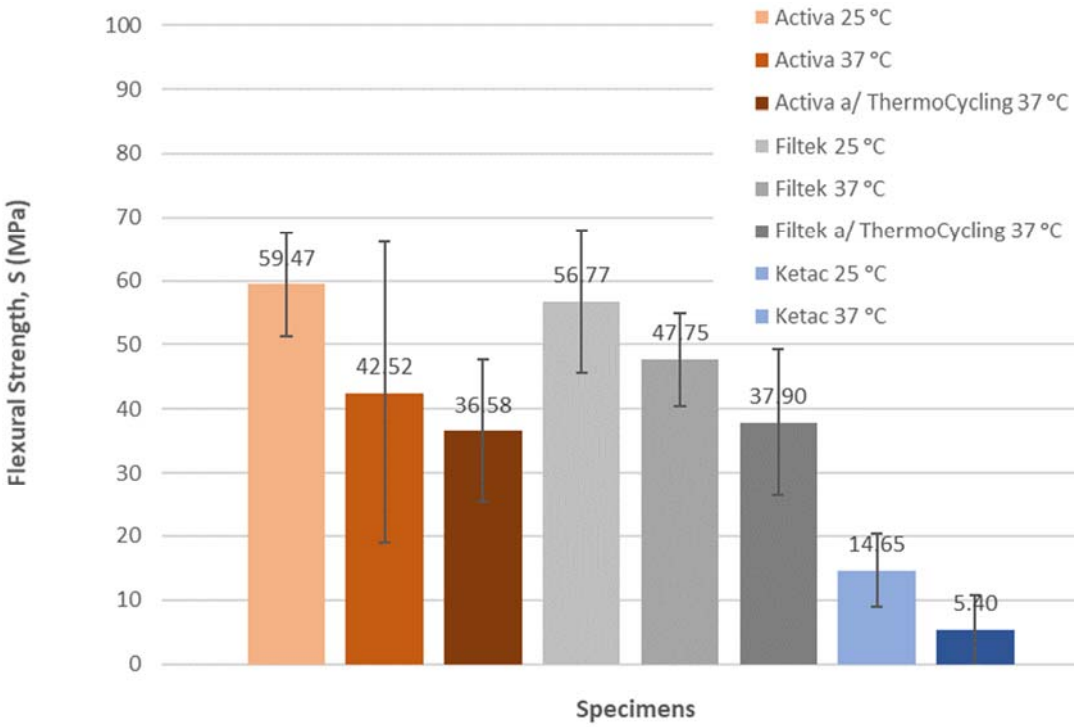

Figure 6. Flexural strength for the different specimens before (25 ± 2 °C and 37 ± 2 °C) and after thermocycling (37 ± 2 °C).

Regarding the results of the static elastic modulus (E_s), presented in Figure 7, and determined through the flexural test, they show similar values to those determined through the impulse excitation of vibration technique and Ketac™ before (25 ± 2 °C and 37 ± 2 °C) and after thermocycling (37 ± 2 °C).

The work of fracture (WOF) is illustrated in Figure 8. Activa™ had a higher fracture toughness than Filtek Supreme™, regardless of temperature and whether it had been subjected to thermocycling or not. Filtek Supreme™ had a resistance to fracture higher than Ketac™, at 25 °C and 37 °C. It was not possible to determine the WOF value for Ketac™ after thermocycling at 37 °C, since the samples broke immediately at the minimum displacement.

3.4. Dynamic Young's Modulus

At 25 °C the results were similar to those of the hardness evaluation, with Activa™ showing a lower E_d (8.03 GPa) than Filtek Supreme™ (12.48 GPa), and Ketac™ having the highest E_d (26.69 GPa).

For Activa™ and Filtek Supreme™, before thermocycling (from 25 °C to 37 °C), there was a variation from 8.03 GPa to 7.91 GPa (1.49%) for Activa™ and from 12.48 GPa to 12.63 GPa (1.20%) for Filtek Supreme™. However, the effect of thermocycling decreased E_d from 7.91 GPa to 6.36GPa (19.60%) for Activa™, and from 12.63 GPa to 9.03GPa (28.50%) for Filtek Supreme™. As for Ketac™, it was not possible to measure the dynamic elastic modulus after thermocycling, since the samples broke immediately when an attempt was

made at measuring by the impulse excitation of vibration technique. The dynamic elastic modulus was significantly different between materials, at 25 °C and after thermocycling ($p < 0.05$) but at 37 °C there was no differences between materials ($p = 0.05$). It was observed that Activa™ had the lowest E_d value, whereas Ketac™ had the highest value (Figure 9).

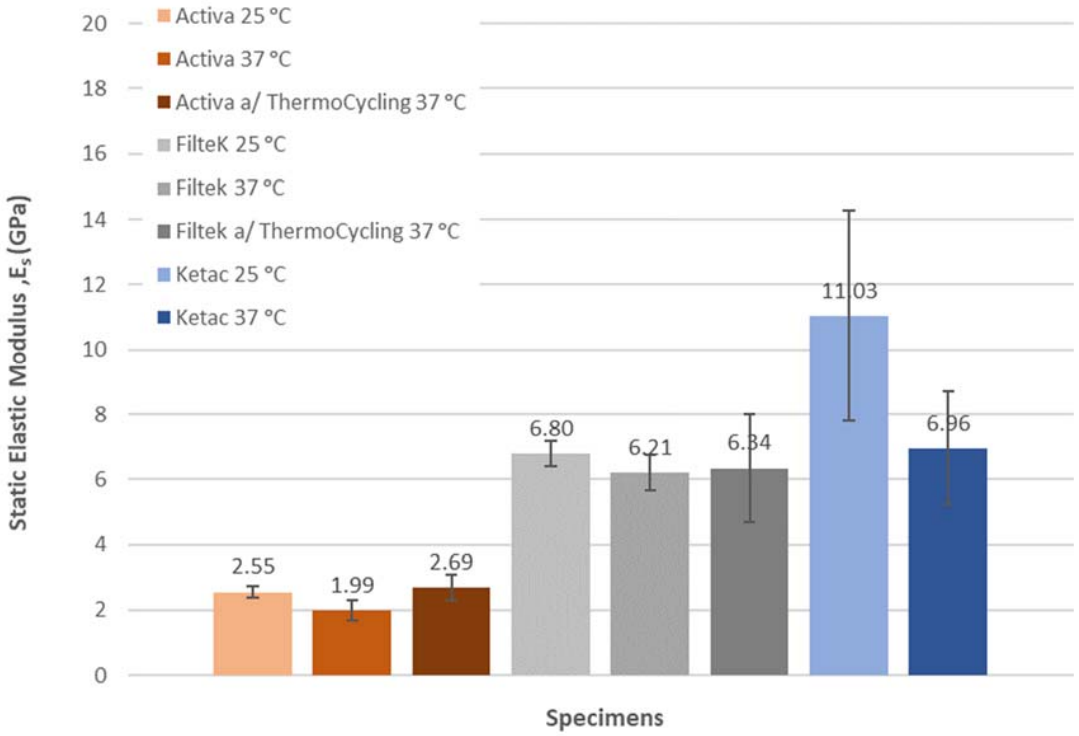

Figure 7. Static elastic modulus for the different specimens before (25 ± 2 °C and 37 ± 2 °C) and after thermocycling (37 ± 2 °C).

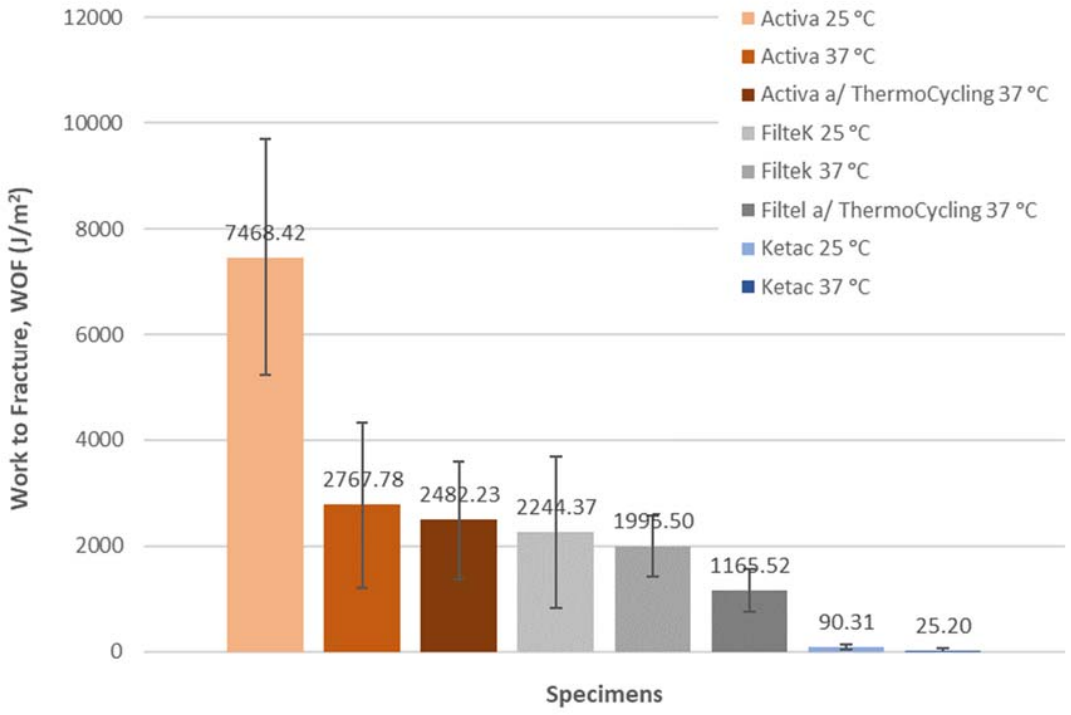

Figure 8. Work of fracture for the different specimens before (25 ± 2 °C and 37 ± 2 °C) and after thermocycling (37 ± 2 °C).

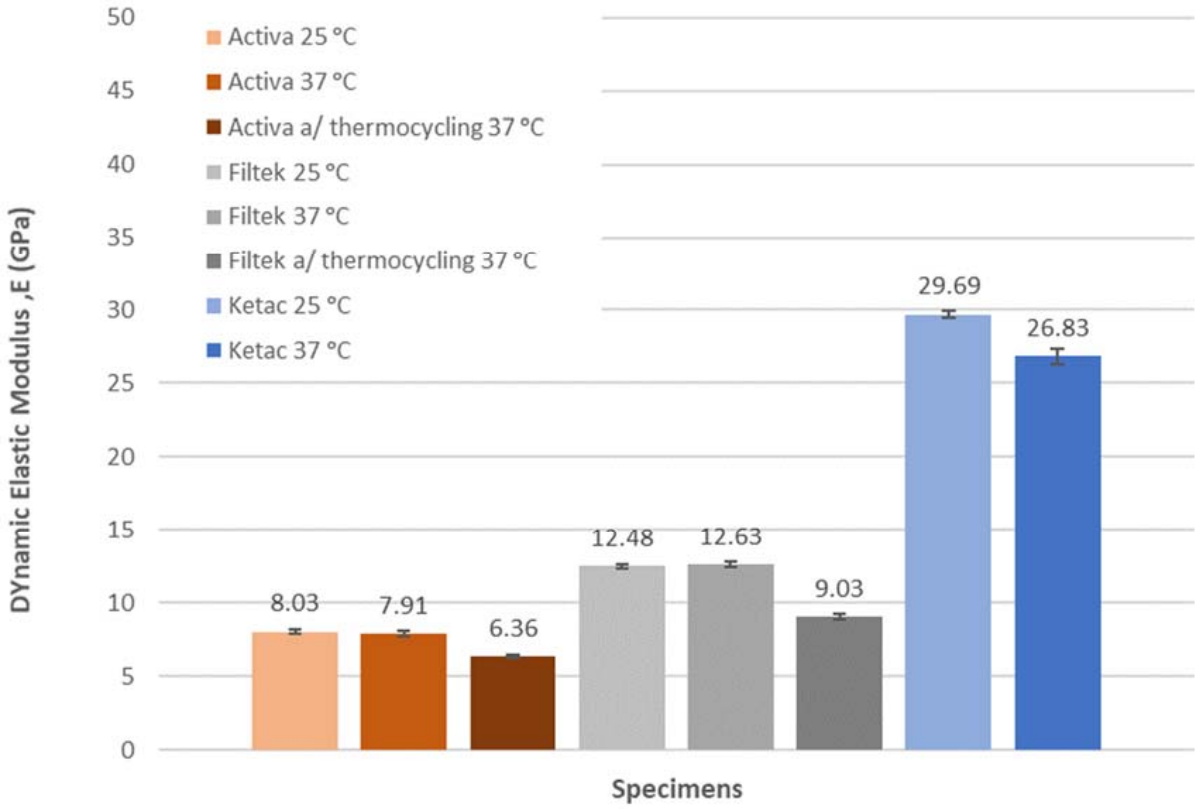

Figure 9. Dynamic elastic modulus for the different materials before (25 ± 2 °C and 37 ± 2 °C) and after thermocycling (37 ± 2 °C).

The ratio of the loss modulus to storage modulus (E''/E') in a viscoelastic material is defined as the tan δ, which provides a measure of damping in the material or degree of energy dissipation, presented in Table 2.

Table 2. tan δ—ratio of the loss modulus to storage modulus for the different specimens (37 ± 2 °C).

Specimens	tan δ
Activa™	0.06
Filtek™	0.044
Ketac™	0.02

3.5. Tribological Characterization

Activa™ was able to better reduce the vibration response with a consequent structure resistance, while Ketac™ showed an opposite behavior which is presented in the graphs in Figure 10.

Figure 9 presents different parts of the scratch test for the Filtek Supreme™ specimen where it is possible to observe the middle part (Figure 10a) and the final part (Figure 10b). It is equally possible to observe the region where the wear profiles were taken (Figure 10a).

Figure 11 shows the wear profiles for the different specimens, before and after thermocycling, showing the evolution of the wear depth and worn area with the transversal distance at a fixed sliding distance of 8 mm (16 N). The depth of the wear track and the worn area are smaller for the Activa™ specimen with values of 98.04 µm and 1.11×10^{-4} µm^2, respectively. For the Filtek Supreme™ specimen, these values increase to 108.32 µm and 1.35×10^{-4} µm^2, respectively. Finally, for the Ketac™ specimen, the values increase signifi-

cantly to 124.71 μm and 2.68 × 10^{-4} μm^2, respectively. For Activa™ and Filtek Supreme™, the results for the worn area and maximum depth of the wear track do not vary much before and after being subjected to thermocycling. In the case of Ketac™ the values obtained for the maximum depth of the wear track before and after thermocycling are 124.71 μm and 203.42 μm, respectively, and the values for the worn area before and after thermocycling are 2.68 × 10^{-4} μm^2 to 3.90 × 10^{-4} μm^2, respectively.

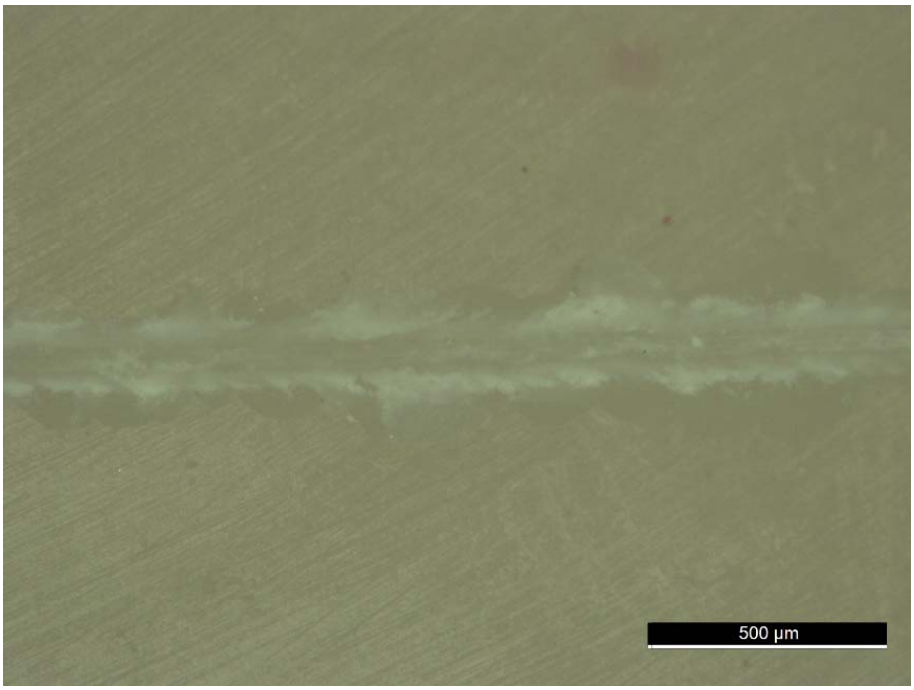

(**a**)

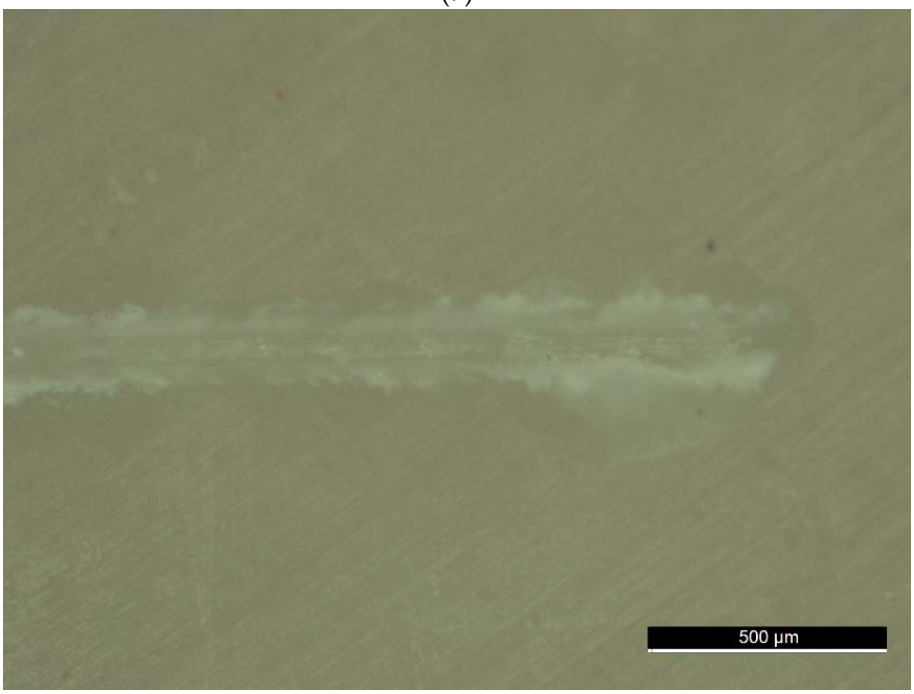

(**b**)

Figure 10. Optical micrographs showing different parts of the longitudinal wear track for the Filtek Supreme™ specimen after thermocycling: (**a**) middle of the scratch and (**b**) end of the scratch.

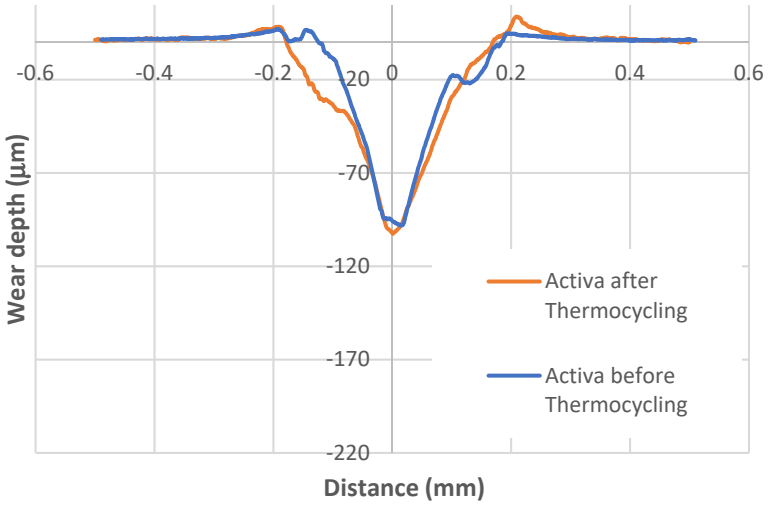

(**a**)

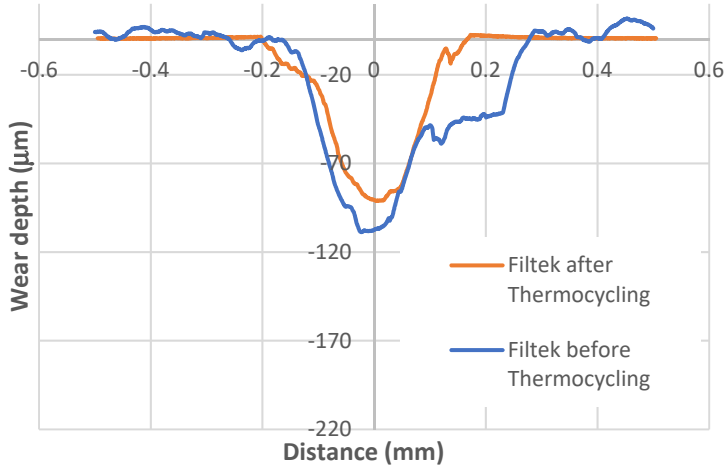

(**b**)

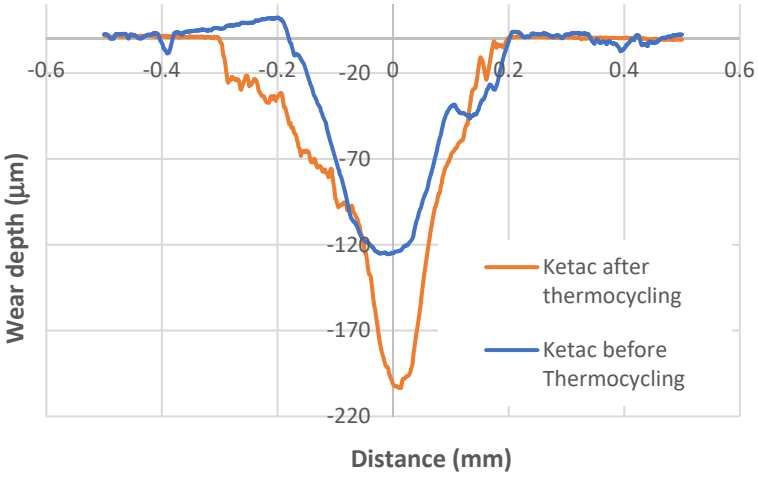

(**c**)

Figure 11. Wear profiles for the different specimens, before and after thermocycling, showing the evolution of the wear depth with the transversal distance. These profiles were taken at 8 mm sliding distance and with an applied load of approximately 16 N: (**a**) Activa™; (**b**) Filtek Supreme™; (**c**) Ketac™.

Figure 12 represents the evolution of the normal force and tangential force with the sliding time. The sliding time is the time it takes the indenter to travel the 10 mm sliding distance. It can be observed that the normal force increases progressively and linearly until reaching approximately 20 N and that the tangential force responds to this force depending on the specimen under analysis. In order to assess the value of the COF for the different specimens, it is necessary to represent the tangential force as a function of the normal force and calculate the slope of the adjusted trend line, as exemplified in Figure 13 for Activa™.

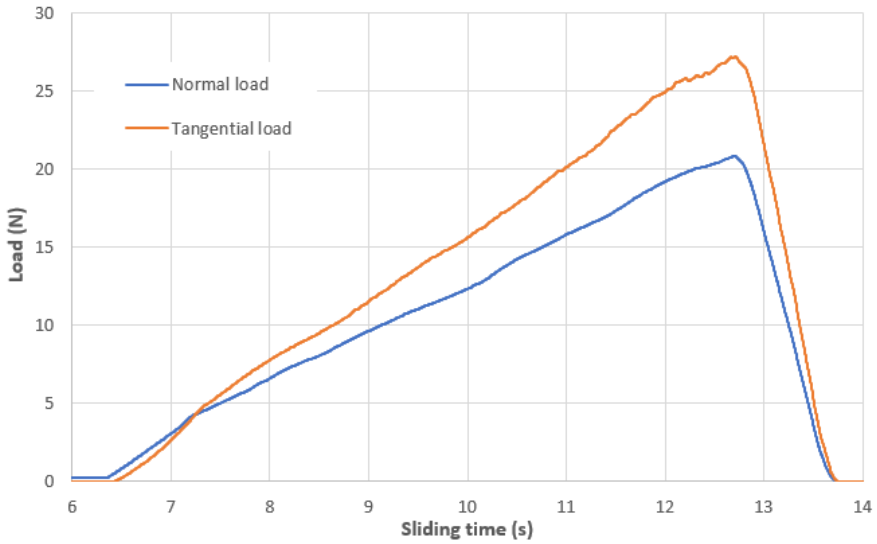

Figure 12. Output from the scratch test, showing the evolution of normal load (blue color) and tangential load (orange color) with sliding time (this test was performed for Activa™ before being subject to thermocycling).

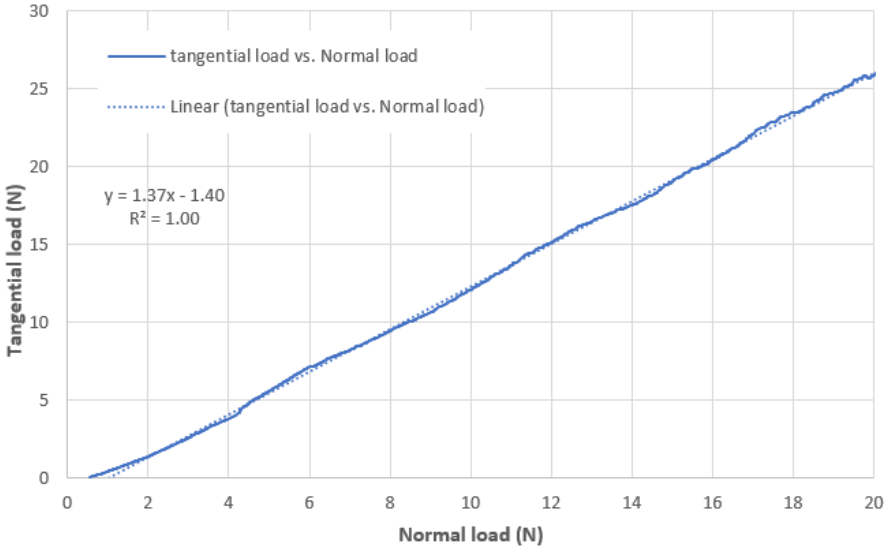

Figure 13. Evolution of the tangential load with normal load showing the slope of the curve (1.37) that matches the value for the COF. This test was performed for the Activa™ specimen before being subject to thermocycling.

Table 3 summarizes the results of the COF as well as the worn area and the maximum depth of the wear track for the different specimens, before and after thermocycling. Regarding the COF, Filtek Supreme™ present lower results than those of the Activa™ and Ketac™. Except for Filtek Supreme™, the COF increased with thermocycling.

Table 3. COF and worn area for the different specimens evaluated during scratch test, before and after thermocycling. The worn area was evaluated at a sliding distance of 8 mm.

		Coefficient of Friction (COF)	Worn Area (μm^2)	Wear Track Maximum Depth (μm)
Activa	**Before**	1.38	1.11×10^{-4}	98.04
	After	1.50	1.35×10^{-4}	102.61
Filtek	**Before**	1.22	2.40×10^{-4}	108.32
	After	1.01	1.57×10^{-4}	91.03
Ketac	**Before**	1.32	2.68×10^{-4}	124.71
	After	1.46	3.90×10^{-4}	203.42

Figure 14 shows SEM micrographs of the wear track for the various specimens before being thermocycled. The wear mechanism was essentially identical before and after thermocycling, which is why micrographs are presented for only one of the cases. The different behavior observed in the indentation track is considerably different for the three materials.

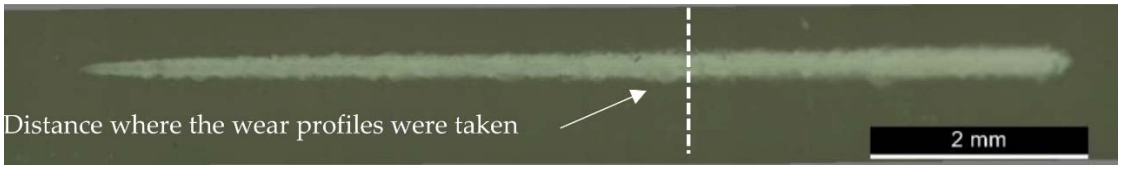

Figure 14. Optical micrograph showing the entire longitudinal wear track for Activa™, before thermocycling.

Figures 15 and 16 show SEM micrographs of the wear track for the various specimens before being thermocycled. It shows that the wear mechanism is essentially identical before and after thermocycling, which is why micrographs are presented for only one of the cases. The different behavior observed in the indentation track is considerably different for the three specimens and is clearly related to the mechanical properties previously measured.

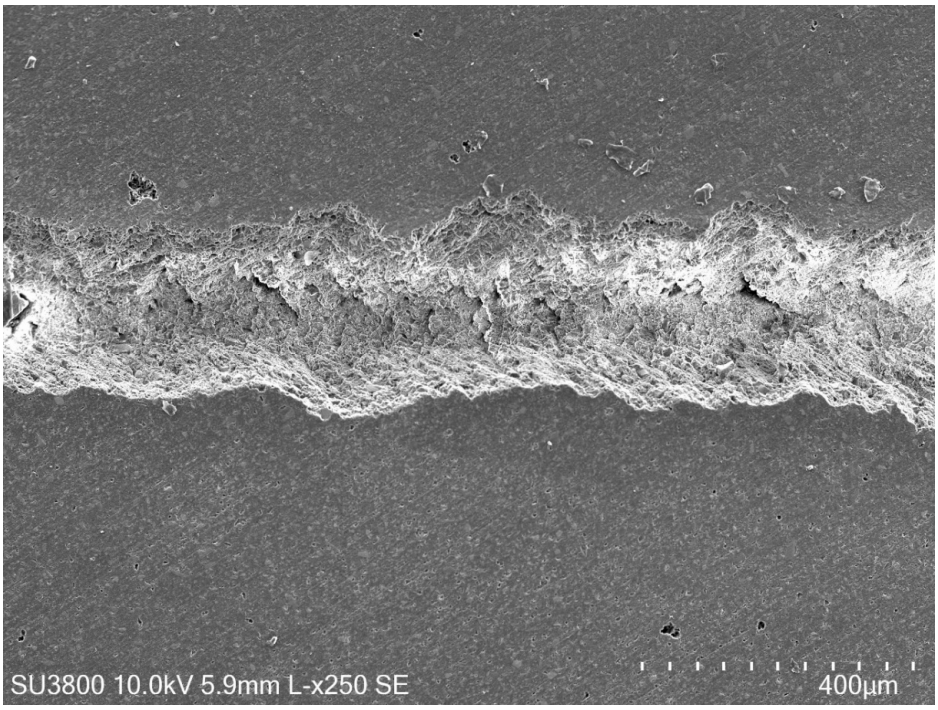

(**a**)

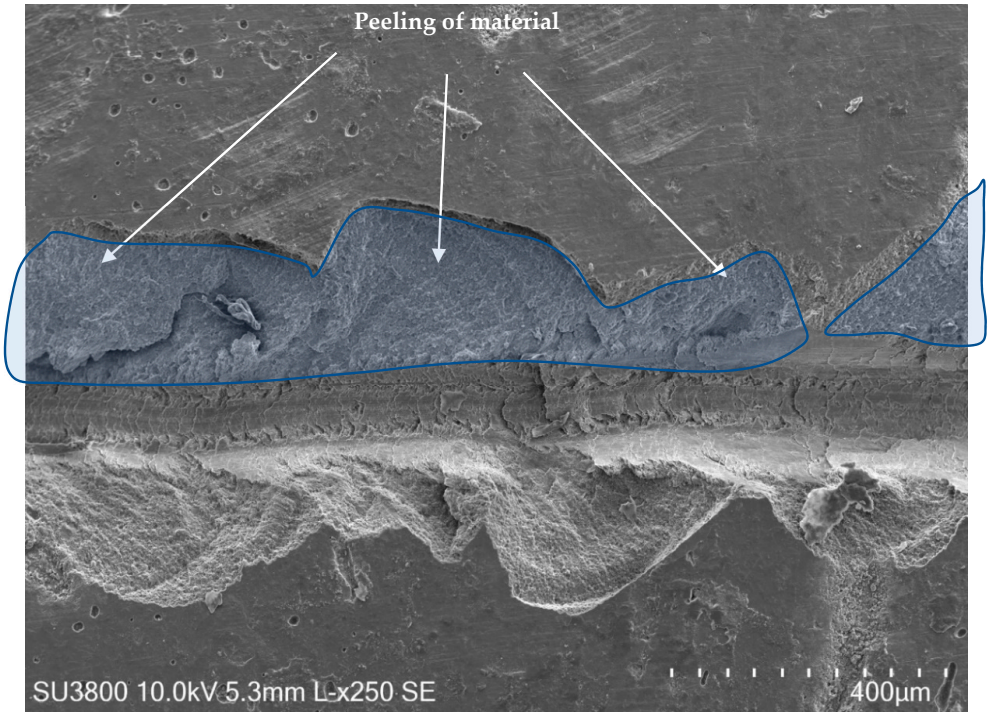

(**b**)

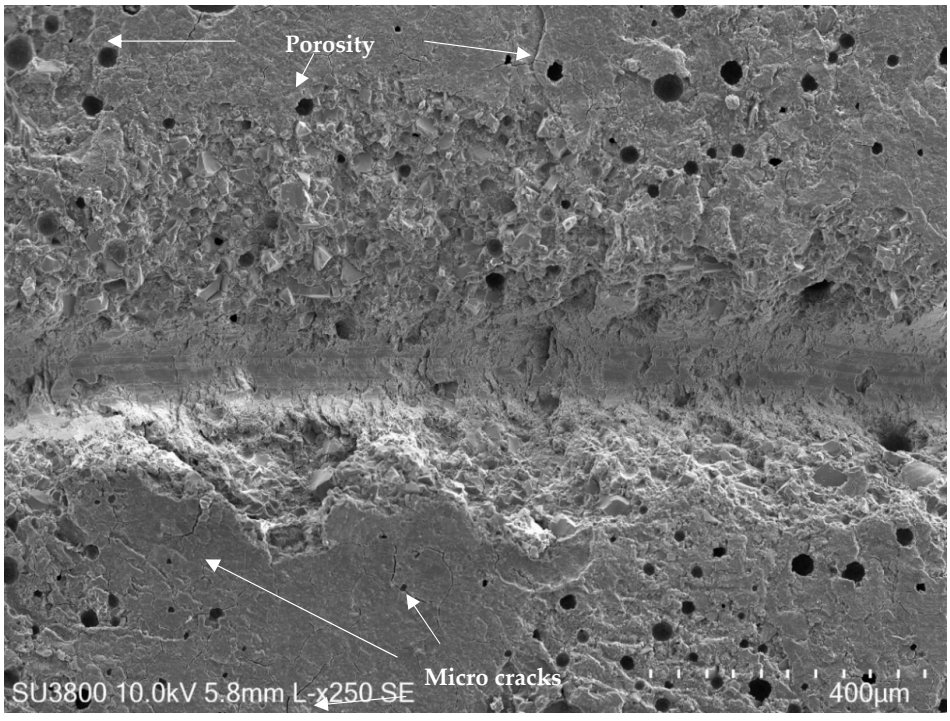

(**c**)

Figure 15. SEM micrographs showing part of the wear track made by scratch tribotesting before thermocycling, for the following specimens: (**a**) Activa™; (**b**) Filtek Supreme™ XTE and (**c**) Ketac™.

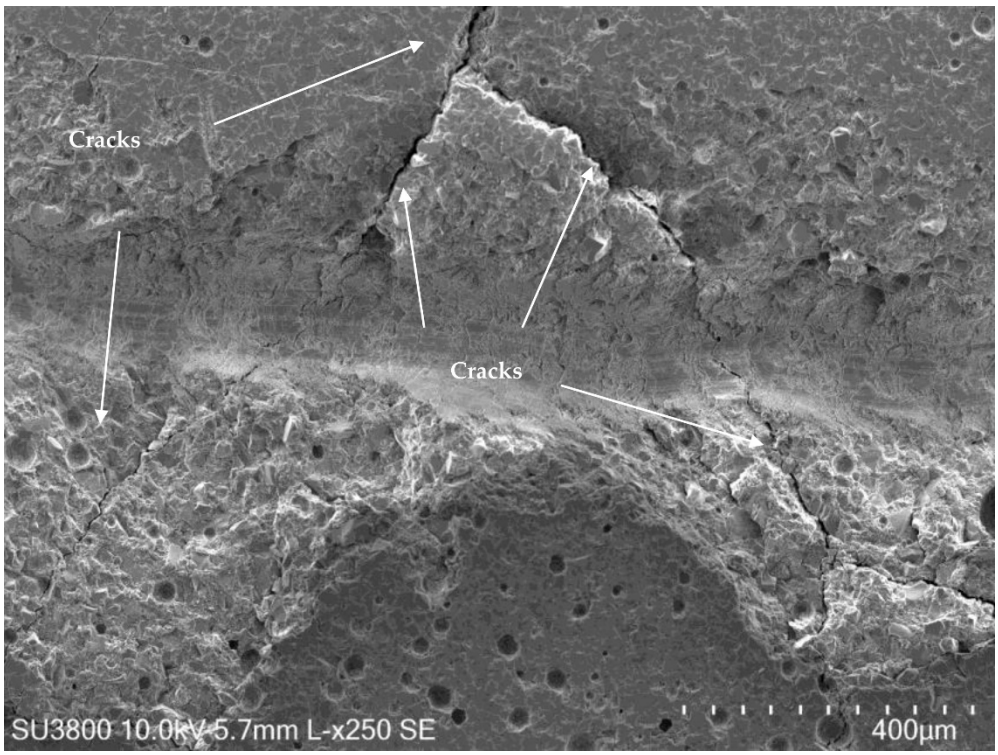

Figure 16. SEM micrograph showing part of the wear track made by scratch tribotesting, for Ketac™ after thermocycling.

3.6. Thermocycling

Before and after thermocycling, statistically significant differences were only found for Ketac™ concerning microhardness ($p = 0.008$) and R_a ($p = 0.043$). For the other measured parameters and materials, no statistically significant differences were found.

4. Discussion

In this experimental study, several mechanical and tribological parameters of Activa™ Bio-active Restorative™, Filtek Supreme™ XTE and Ketac™ Fil Plus Aplicap™ were tested.

The oral temperature changes were simulated by undertaking thermocycling for half of the samples included in each study group. Thermocycling results in surface stresses and interface microcracks due to high thermal gradients, so it can assess material stability and filler/matrix interaction [19].

The variability of the composition of restorative materials influences its physical parameters, such as flexural strength, fracture toughness, Vickers hardness, elastic modulus, and curing depth, among others [20]. The diffusion of water molecules that occur in the polymer matrix when dental restorations are in contact with saliva can compromise their physical and mechanical properties [12].

Ketac™ exhibited the highest microhardness and a significant decrease of its values after thermocycling was found, which makes it an unstable material. Although Filtek™ XTE and Activa™ were associated with lower microhardness values before thermocycling, no significant differences were found before and after thermocycling. As such, this material may be considered the most stable in terms of hardness. These results are in accordance with the investigation of Alrahlah et al. [4], who also evaluated the microhardness of Activa™ and Ketac™ before and after thermocycling.

The arithmetic average of the absolute heights (R_a) and the mean square root of the height of profiles (R_q) were selected since these roughness measurements are widely used and allow the comparison of sample roughness concerning their esthetic aspects [21,22]. Ketac™ was the only material that presented statistically significant differences in R_a after

thermocycling, which is in accordance with the results of previous studies [23,24]. This increase in surface roughness, observed in glass-ionomer specimens, can determine the increase in bacterial adhesion and infiltration, allowing fast microbial colonization [23,24]. R_z, the average distance between the highest peak and lowest valley in each sampling length, enables an idea of the profile's total height [21,22]. The differences found between Filtek™ and Activa™, regarding this parameter, could be due to the fact that nanohybrid composites have nanofillers and micrometer particles (0.4–5 µm) in their composition [25].

The only parameter that did not vary significantly with thermocycling was the skewness (R_{sk}), which is related to the surface load capability. A negative value of R_{sk} indicates that there are valleys in the surface [21,22]. Therefore, the general observed trend of an increase in the R_{sk} values was correlated with a decrease in the superficial pores by swelling induced by the thermocycling. There was a decrease in all groups, except for Filtek Supreme™, but the differences were not statistically significant. This fact was corroborated by Carreira et al. who reported a decrease in R_{sk} values of a nanohybrid composite after thermocycling [12]. According to Ţălu et al. [26], a negative R_{sk} shows the positive load-resistance ability of the surface of dental restorative materials, which would have a relatively stable wear rate during function. Regarding the 2D roughness parameters, it is difficult to draw precise conclusions as the final surface was identical for all specimens and that this difference is due to the type of microstructure that makes up the different specimens.

Wear resistance of a dental material is a prerequisite to its acceptance by both dentists and patients. A high level of resistance may contribute to its durable esthetics and longevity. This is an important factor to be considered when selecting restorative materials for clinical use as many variables that derive from their composition directly influence their wear resistance [20].

The properties of dental composites depend on various factors related to the filler particles, the polymeric matrix and the coupling between matrix and filler [27,28]. Filtek™ Supreme™ contains bis-GMA, UDMA, bis-EMA and a low quantity of TEGDMA resins [29]. Activa™ results from a mixture of UDMA and other methacrylates with modified polyacrylic acid [30]. Ketac™ results from a mixture of calcium fluoro-alumino-silicate glass powder and an aqueous solution with the copolymer of polyacrylic acid-itaconic acid and tartaric acid [31]. Regarding the composition of the studied materials, the results are in line with those of Asmussen et al. [27]. The authors reported that a composite resin with a high percentage of UDMA (~70 mol%), a low percentage of TEGDMA (~30 mol%) and no Bis-GMA would result in optimum strength. Such a material would present a relatively low elastic modulus of about 8 GPa [27]. According to this investigation, Activa™ obtained an initial elastic modulus of 8.03 ± 0.15 GPa, followed by Filtek Supreme™ (12.48 ± 0.18 GPa) and finally Ketac™ (26.69 ± 0.26 GPa). The elastic modulus provides an idea about the rigidity of the material. The higher the value of the elastic modulus, the greater the stress required for the same degree of deformation, and therefore the more rigid the material.

Flexural strength (FS) is one of the key mechanical properties selected by the International Organization for Standardization (ISO) for screening of resin-based materials [5]. The fracture properties of materials are determined by their FS and are critical if the material is used for filling dental cavities [28]. Surface characteristics of restorative materials may affect FS [32]. In this investigation, Activa™ had the highest fracture toughness, followed by Filtek Supreme™ and Ketac™, regardless of temperature and whether it had been subjected to thermocycling. These facts corroborate the results obtained in the tribological tests, where a large number of cracks could be observed through an SEM micrograph for Ketac™ after thermocycling, which weakened the integrity of the specimen after testing. Some studies report that flexural strength increases when bis-GMA or TEGDMA are substituted by UDMA [27,33], which could justify the highest FS of Activa™. These materials, which the manufacturer reports as containing a resilient resin matrix with energy-absorbing elastomeric components (diurethane and methacrylates with modified polyacrylic acid and polybutadiene modified diurethane dimethacrylate), may be more suitable in higher-stress

areas that are contraindicated for conventional glass-ionomer cements [7]. According to the existing literature, FS values for conventional resin-modified glass-ionomer cement (RMGIC) materials range from 42 MPa to 66 MPa, 25 MPa to 60 MPa, and 16.9 MPa to 59 MPa [23]. In a study by Pameijer et al. [5], the FS of RMGIC was found to be greater than the one of conventional composite resin materials. In addition, bioactive RMGIC showed a higher FS than that of conventional glass-ionomer cements (Fuji™, Ketac™) [5]. Thus, the results from this study are in accordance with the available literature. The difference in the FS of the tested materials may be attributed to the difference in their composition, type of resin, inorganic filler, and size and content of the fillers [34].

Activa™ had a homogeneous wear track where no cracks were visible outside the wear track and where the track width was approximately constant. This fact may be related to the low hardness value obtained in the Vickers test (HV0.2 = 20.2 Kgf/mm^2), which allows the removal of material, but at the same time a high fracture toughness as evidenced in the calculated value of work of fracture (WOF = 2767.78 J/m^2) which maintains the integrity of the composite. This wear track with a smooth surface and without visible cracks is characteristic of a ductile removal mode.

Filtek Supreme™ had a very irregular wear track, as a consequence of the constant peeling of material that was visible in a perpendicular direction to the wear track. This peeling explains the wider wear profiles and it was noticeable that fragments or portions of large amounts of material came out. This fact can be related to the moderate hardness obtained in the Vickers test (HV0.2 = 67.7 Kgf/mm^2) and with the work of fracture value (WOF = 1995.50 J/m^2). The observed scratch wear track where brittle peeling of great portions of material was observed is characteristic of brittle removal mode.

Ketac™ showed a very wide wear track where a destruction of the material on the edges of the wear track could be observed with large cracks that extended in all directions. This fact can be related to the high hardness obtained in the Vickers test (HV0.2 = 110.65 Kgf/mm^2) and the very low value of fracture toughness that is related to the determined value of work of fracture (WOF = 25.20 J/m^2). The existence of high porosity also helps to understand the properties observed. Furthermore, it was observed that, after thermocycling, Ketac™ showed the same wear mechanism, but a considerable increase in the number of fractures could be observed in various directions. This fact can be explained by the increased hardness and decreased fracture toughness after thermocycling.

Although this study allows for a better understanding of the mechanical and tribological properties of dental restorative materials, it has some limitations. The test methods vary among authors and, therefore, it was difficult to compare results to the ones of similar works. Although the experimental procedures incorporate a multi-parametric analysis, the number of specimens per group could have been higher to promote more accurate results. In addition, the WOF for Ketac™ after thermocycling at 37 °C could not be determined, since the samples broke immediately at the minimum displacement.

5. Conclusions

During the present research work, it was possible to conclude that:

- The four-point flexural test and scratch testing are expeditious methods to determine the mechanical and tribological properties of newly developed composite resins for restorative dentistry.
- Of all the composites analyzed, Activa™ was the one with the lowest hardness, followed by Filtek™ and consequently Ketac™. However, toughness presented the inverse order, with Activa™ showing greater resistance to fracture than Filtek™ and in turn than Ketac™.
- The stiffness or elastic modulus determined by the two different methods show the same trend although with different amplitudes.
- For the tribological test an increasing normal load up to 20 N was applied. A COF varying between 1 and 1.5 was observed with the maximum value for the Activa

specimen and the minimum value for Filtek™. Regarding the wear rate, this was lower for Activa™, followed by Filtek™ and Ketac™.

- Related with the wear mechanism it was shown that Activa™ presented a smooth surface without visible cracks characteristic from a ductile removal mode, while Filtek™ and Ketac™ presented a brittle peeling of great portions of material characteristic of brittle removal mode.
- Activa™ can absorb impact better than Filtek™ and Ketac™.

Activa™ performed better in relation to fracture toughness, wear rate and impact absorption than Filtek™ and Ketac™. Moreover, thermocycling had little effect on this bioactive composite.

Further studies are needed, with standardized protocols, to establish clear relations between the evaluated parameters for each material and to confirm their clinical performance.

Author Contributions: Conceptualization, L.V., A.R. and E.C.; methodology, A.S.C., L.V., A.R. and E.C.; software, E.R.C., A.S.C. and L.V.; validation, A.S.C., M.M.F., L.V., A.R. and E.C.; formal analysis, E.R.C., A.S.C., L.V., A.R. and E.C.; investigation, E.R.C., A.S.C., I.A., A.B.P., C.M.M. and J.S.; data curation, E.R.C., A.S.C., I.A., L.V., A.R. and E.C.; writing—original draft preparation, E.R.C., A.S.C., I.A., A.B.P., C.M.M., L.V. and J.S.; writing—review and editing, A.S.C., I.A., M.M.F., L.V., A.R. and E.C.; supervision, L.V., A.R. and E.C. All authors have read and agreed to the published version of the manuscript.

Funding: This research received no external funding.

Institutional Review Board Statement: Not applicable.

Informed Consent Statement: Not applicable.

Conflicts of Interest: The authors declare no conflict of interest.

References

1. Francisconi, L.F.; Mendes Candia Scaffa, P.; dos Santos Paes de Barros, V.R.; Coutinho, M.; Silveira Francisconi, P.A. Glass ionomer cements and their role in the restoration of non-carious cervical lesions. *J. Appl. Oral Sci.* **2009**, *17*, 364–369. [CrossRef]
2. Jefferies, S.R. Bioactive and biomimetic restorative materials: A comprehensive review. Part I. *J. Esthet. Restor. Dent.* **2014**, *26*, 14–26. [CrossRef]
3. El-Banna, A.; Sherief, D.; Fawzy, A.S. Resin-based dental composites for tooth filling. In *Advanced Dental Biomater.*; Khurshid, Z., Najeeb, S., Zafar, M.S., Sefat, F., Eds.; Woodhead Publishing: Cambridge, UK, 2019; pp. 127–173. [CrossRef]
4. Alrahlah, A. Diametral tensile strength, flexural strength, and surface microhardness of bioactive bulk fill restorative. *J. Contemp. Dent. Pract.* **2018**, *19*, 13–19. [CrossRef] [PubMed]
5. Pameijer, C.H.; Garcia-Godoy, F.; Morrow, B.R.; Jefferies, S.R. Flexural strength and flexural fatigue properties of resin-modified glass ionomers. *J. Clin. Dent.* **2015**, *26*, 23–27. [PubMed]
6. Amaireh, A.I.; Al-Jundi, S.H.; Alshraideh, H.A. In vitro evaluation of microleakage in primary teeth restored with three adhesive materials: ACTIVA™, composite resin, and resin-modified glass ionomer. *Eur. Arch. Paediatr. Dent.* **2019**, *20*, 359–367. [CrossRef] [PubMed]
7. Pulpdent Co. Activa (Bioactive Restorative Material) Pamphlet. Available online: https://www.pulpdent.com/activa-bioactive-white-paper/ (accessed on 12 July 2021).
8. Croll, T.P.; Berg, J.H.; Donly, K.J. Dental repair material: A resin-modified glass-ionomer bioactive ionic resin-based composite. *Compend. Contin. Educ. Dent.* **2015**, *36*, 60–65.
9. ElReash, A.A.; Hamama, H.; Abdo, W.; Wu, Q.; Zaen El-Din, A.; Xiaoli, X. Biocompatibility of new bioactive resin composite versus calcium silicate cements: An animal study. *BMC Oral Health* **2019**, *19*, 1–10. [CrossRef]
10. Davidson, C.L. Advances in glass-ionomer cements. *J. Appl. Oral Sci.* **2006**, *14*, 3–9. [CrossRef]
11. Antunes, P.V.; Ramalho, A.; Carrilho, E.V.P. Mechanical and wear behaviours of nano and microfilled polymeric composite: Effect of filler fraction and size. *Mater. Des.* **2014**, *61*, 50–60. [CrossRef]
12. Carreira, M.; Antunes, P.V.; Ramalho, A.; Paula, A.; Carrilho, E. Thermocycling Effect on Mechanical and Tribological Characterization of Two Indirect Dental Restorative Materials. *J. Braz. Soc. Mech. Sci. Eng.* **2017**, *39*. [CrossRef]
13. *E384. Standard Test Method for Microindentation Hardness of Materials, Developed by Subcommittee: E04.05, Book of Standards Vol 03.01*; ASTM: West Conshohocken, PA, USA, 2010.
14. EN ISO-4287. *Geometrical Product Specifications (GPS)—Surface Texture: Profile Method—Terms, Definitions and Surface Texture Parameters*; International Organization for Standardization (ISO): Geneva, Switzerland, 1997; pp. 1–25.
15. ASTM D6272-02. *Standard Test Method for Flexural Properties of Unreinforced and Reinforced Plastics and Electrical Insulating Materials by Four-Point Bending*; ASTM International: West Conshohocken, PA, USA, 2002.

16. ASTM E1876-01. *Standard Test Method for Dynamic Young's Modulus, Shear Modulus, and Poisson's Ratio by Impulse Excitation of Vibration*; ASTM International: West Conshohocken, PA, USA, 2006.
17. Carvalho, A.L.; Vilhena, L.M.; Ramalho, A. Study of the frictional behavior of soft contact lenses by an innovative method. *Tribol. Int.* **2021**, *153*. [CrossRef]
18. ASTM G171. *Standard Test Method for Scratch Hardness of Materials Using a Diamond Stylus*; ASTM: West Conshohocken, PA, USA, 2009; Volume 3, pp. 1–7.
19. Chadwick, R.G.; McCabe, J.F.; Walls, A.W.; Storer, R. The effect of storage media upon the surface micro-hardness and abrasion resistance of three composites. *Dent. Mater.* **1990**, *6*, 123–128. [CrossRef]
20. Heintze, S.D.; Zellweger, G.; Zappini, G. The relationship between physical parameters and wear of dental composites. *Wear* **2007**, *263*, 1138–1146. [CrossRef]
21. Neto, J. *Metrologia e Controle Dimensional*, 1st ed.; Elsevier: Amsterdam, The Netherlands, 2012.
22. Gadelmawla, E.S.; Koura, M.M.; Maksoud, T.M.A.; Elewa, I.M.; Soliman, H.H. Roughness parameters. *J. Mater. Process. Tech.* **2002**, *123*, 133–145. [CrossRef]
23. Hamouda, I.M. Effects of various beverages on hardness, roughness, and solubility of esthetic restorative materials. *J. Esthet. Restor. Dent. Off. Publ. Am. Acad. Esthet. Dent.* **2011**, *23*, 315–322. [CrossRef] [PubMed]
24. Ellakuria, J.; Triana, R.; Mínguez, N.; Soler, I.; Ibaseta, G.; Maza, J.; García-Godoy, F. Effect of one-year water storage on the surface microhardness of resin-modified versus conventional glass-ionomer cements. *Dent. Mater.* **2003**, *19*, 286–290. [CrossRef]
25. Chen, M.-H. Update on dental nanocomposites. *J. Dent. Res.* **2010**, *89*, 549–560. [CrossRef] [PubMed]
26. Ţălu, Ş.; Stach, S.; Lainović, T.; Vilotić, M.; Blažić, L.; Alb, S.F.; Kakaš, D. Surface roughness and morphology of dental nanocomposites polished by four different procedures evaluated by a multifractal approach. *Appl. Surf. Sci.* **2015**, *330*, 20–29. [CrossRef]
27. Asmussen, E.; Peutzfeldt, A. Influence of UEDMA, BisGMA and TEGDMA on selected mechanical properties of experimental resin composites. *Dent. Mater.* **1998**, *14*, 51–56. [CrossRef]
28. Ersoy, M.; Civelek, A.; L'Hotelier, E.; Say, E.C.; Soyman, M. Physical properties of different composites. *Dent. Mater. J.* **2004**, *23*, 278–283. [CrossRef] [PubMed]
29. Products MED. Technical Product Profile: Filtek Supreme XTE. 2010. Available online: www.Multimedia.3m.Com (accessed on 12 July 2021).
30. Products MED. Technical Product Profile: ActivaTM BioActive White Paper. 2019. Available online: www.Pulpdent.Com (accessed on 12 July 2021).
31. Products MED. Technical Product Profile: KetacTM Universal AplicapTM. 2012. Available online: www.Multimedia.3m.Com (accessed on 12 July 2021).
32. Kawano, F.; Ohguri, T.; Ichikawa, T.; Matsumoto, N. Influence of thermal cycles in water on flexural strength of laboratory-processed composite resin. *J. Oral Rehabil.* **2001**, *28*, 703–707. [CrossRef] [PubMed]
33. Ogliari, F.A.; Ely, C.; Zanchi, C.H.; Fortes, C.B.; Samuel, S.M.; Demarco, F.F.; Petzhold, C.L.; Piva, E. Influence of chain extender length of aromatic dimethacrylates on polymer network development. *Dent. Mater.* **2008**, *24*, 165–171. [CrossRef] [PubMed]
34. Floyd, C.J.; Dickens, S. Network structure of Bis-GMA-and UDMA-based resin systems. *Dent. Mater.* **2006**, *22*, 1143–1149. [CrossRef] [PubMed]